arXiv:1502.04546v1 [physics.optics] 16 Feb 2015

Control of optical spin Hall shift in phase-discontinuity metasurface by weak value measurement post-selection

Y.U. Lee and J.W. Wu*

Department of Physics and Quantum Metamaterials Research Center
Ewha Womans University, Seoul 120-750, Korea

*jwwu@ewha.ac.kr

Optical spin Hall (OSH) shift has been observed by weak measurement amplification in a refraction beam passing through air-glass interface, the refractive index gradient $\vec{\nabla}n$ being normal to the interface. [1] Phase-discontinuity metasurface (PMS) possesses $\vec{\nabla}n$ tangential to the metasurface, and depending on the incidence angle either positive or negative refraction takes place satisfying the generalized Snell's law. [2] Rapid phase-change over subwavelength distance at PMS leads to a large $\vec{\nabla}n$, enabling a direct observation of OSH shift. [3] Here, we identify that the relative OSH shift between optical beams with spins ± 1 depends on incidence and refraction angles at PMS, and demonstrate a control of OSH shift by constructing a weak value measurement with a variable phase retardance in the post-selection. Capability of OSH shift control permits a tunable precision metrology applicable to nanoscale photonics such as angular momentum transfer and sensing.

OSH effect is attributed to spin-orbit interaction of light in an optical beam propagating along a curved trajectory, originating from the transversality nature of electromagnetic field. [4, 5] When a linearly polarized beam refracts at the interface of two optical media, optical beams with spins ± 1 experience an OSH transverse spatial shift in opposite directions. [6, 7] In a PMS composed of an array of V-shaped antennae, a large amount of refraction takes place in cross-polarized scattering light over subwavelength distance, leading to an OSH shift in extraordinary refraction beam in the order of a few hundreds nanometers at the near IR spectral range. [3]

One distinct feature of PMS is that the refractive index gradient is tangential to the metasurface, differently from air-glass interface where the refractive index gradient is normal to the interface. At the air-glass interface shown in Fig. 1(a), the radii of equifrequency surfaces are different in air and glass, and transverse shifts cancel out at top and bottom interfaces possessing opposite refractive index gradients. [1]. At PMS on a glass, on the other hand, the net transverse shift comes from the refractive index gradient of metasurface as shown in Fig. 1(b) with a single spherical equifrequency surface with the radius specified by the dispersion relation of light in air.

The spin-orbit interaction of light is one example of interaction Hamiltonians coupling heavy/slow and light/fast systems constituting a physical object. Coupling of heavy/slow and light/fast systems leads to effects of action and reaction between the two systems. [7–9] Polarization-plane rotation of light along a coiled optical fiber results from the effect of a curved beam trajectory (slow) on optical spin (fast), which is a manifestation of the Berry phase in the light polarization. [10] On the other hand, the effect of optical spin (fast) on a curved beam trajectory (slow) gives rise to a spin-dependent transverse shift of optical beam centroid, described by the Lorentz force in momentum space, $\lambda\vec{\nabla}n \times \frac{\vec{p}}{p^3}$, where $\frac{\vec{p}}{p^3}$ is the monopole Berry

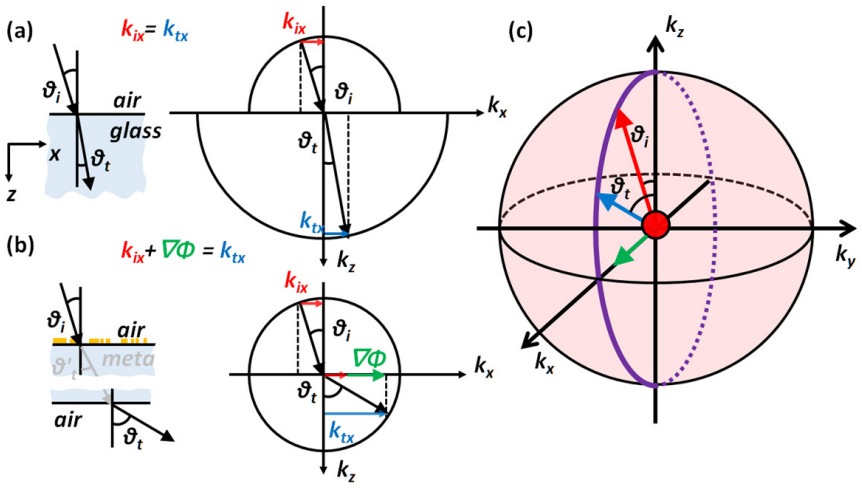


Fig. 1. Schematics of optical beam refractions with refractive index gradient $\vec{\nabla}n$ in the incidence plane is shown. (a) At air-glass interface $\vec{\nabla}n$ is along z-axis normal to the surface, and radii of equifrequency surfaces are different in air and glass (b) At phase-discontinuity metasurface $\vec{\nabla}n$ is along x-axis tangential to the surface, and the net refraction after passing through the glass substrate is described by equifrequency surface in air with an additional momentum from $\vec{\nabla}\Phi$. (c) 3D plot of incidence (red) and refraction (blue) wavevectors and phase gradient $\vec{\nabla}\Phi$ (green) are shown. Monopole is located at the center of the equifrequency surface.

curvature associated with optical beam of spin λ. [6, 7, 12, 22]

In the equifrequency surface of PMS shown in Fig. 1(c) the refractive index gradient is along x-axis, and the monopole Berry curvatures are radial vectors with directions determined by incidence and refraction angles θ_i and θ_t. Transverse shift δy upon refraction at PMS is related to the phase gradient $\vec{\nabla}\Phi = 2\pi\vec{\nabla}n$ and Berry connections of incidence and refraction beams, yielding the expression of transverse shift: [22, 23]

$$\delta y \quad = \quad -\lambda \frac{\cos\theta_t - \cos\theta_i}{|\vec{\nabla}\Phi|} \,. \tag{1}$$

See SI for derivation of Eq. (1). From the two facts that both positive and negative refractions can take place at PMS and that $\vec{\nabla}n$ is tangential to the PMS surface, the sign and magnitude of transverse shift δy depend on incidence and refraction angles θ_i and θ_t as well as $|\vec{\nabla}\Phi|$, as can be read-off from Fig. 1(c) and Eq. (1).

Figure 2(a) shows examples how the relative transverse shift of optical beams with spins ± 1 changes sign in detail. For $\lambda = +1$ corresponding to the red arrows in Fig. 2(a), when $\theta_i < \theta_t$ a positive transverse shift ($\delta y > 0$) takes place in both positive (①) and negative (②) refractions, and when $\theta_i > \theta_t$ a negative transverse shift ($\delta y < 0$) takes place in both negative (③) and positive (④) refractions. In Fig. 2(b) are plotted theoretical calculation (solid curves) and experimental measurement (solid circles) of refraction angle θ_t and transverse shift δy as a function of incidence angle θ_i.

Weak measurement amplification enabled the observation of OSH shift in air-glass interface. [1] By preparing a polarizer as pre-selection, the weak value is measured by a strong

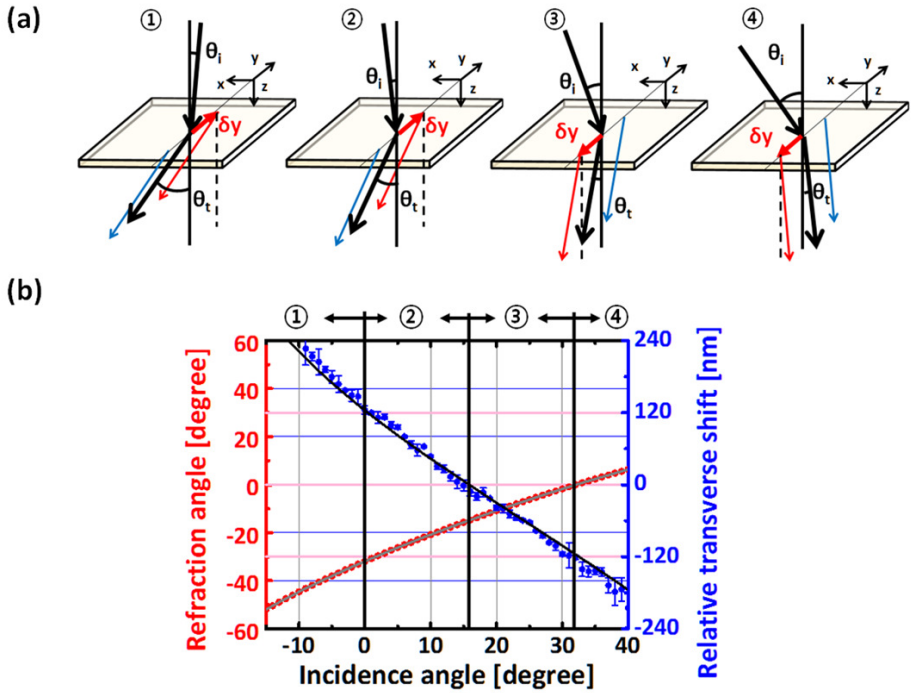


Fig. 2. (a) Schematics of the beam refraction from air to ① a positive-refraction-low-index medium, ② a negative-refraction-low-index medium, ③ a negative-refraction-high-index medium, and ④ a positive-refraction-high-index medium are shown. (b) Theoretical calculation (solid curve) and experimental measurement (solid circle) of refraction angle (red) θ_t and relative transverse shift (blue) are plotted as a function of incidence angle θ_i.

measurement with a nearly cross-polarized analyzer as post-selection. [14] In PMS, on the other hand, OSH shift was directly detected without resorting to a weak measurement amplification. When it is attempted to control the transverse shift in PMS by an optical means, however, a weak value measurement can be utilized with a variable phase retardance in the post-selection.

OSH shift is one example of classical analogues of a quantum measurement of the polarization state of a paraxial beam by its transverse amplitude distribution. [15] By introducing a variable optical phase retardance in the post-selection, we can tune the post-selected state $|\psi_f>$ across the whole range of retardance, $[0, \pi/2]$, to control OSH shift, which is made possible in PMS since OSH shift is large enough to be observed in the optical far field. We place a phase retarder with variable retardance Γ (modulus of π) inside the cross polarizer/analyzer (P_1/P_2) setup in order to control OSH shift in the weak measurement as shown in Fig. 3, where the post-selection state is $|\psi_f(\Gamma)>=\big(\cos(\pi\Gamma), -i\sin(\pi\Gamma)\big)$.

When OSH transverse shift is measured at the propagation distance z of a Gaussian beam with Rayleigh range of z_0, the observable *metaOSH* is expressed in terms of the Pauli matrix $\hat{\sigma}_2$ in the linear polarization bases: [16, 17, 23]

$$metaOSH = -\hat{\sigma}_2 \cdot \delta y \cdot \frac{z}{z_0} \,. \tag{2}$$

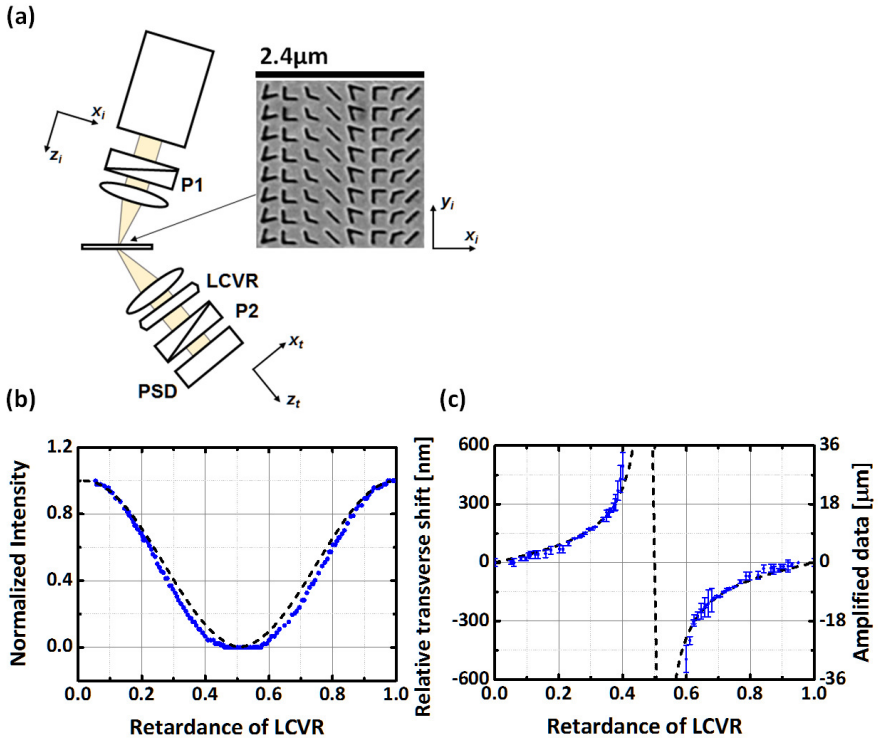


Fig. 3. (a) Schematics of weak measurement with a variable retardance is shown with P_1=(1,0)^T and P_2=(0,1) along with SEM image of Babinet complementary phase-gradient metasurface. [18] LCVR is liquid-crystal variable retarder and PSD is a quadrant position sensitive detector. See Methods for the detailed description of sample and measurement. (b) Light intensity transmitted through a cross polarizer/analyser setup is plotted as a function of retardance Γ of LCVR. (c) Weak value of OSHE shift post-selected with phase retardance is plotted as a function of retardance Γ of LCVR with the corresponding transverse shift. Blue solid circles are data point and dashed curves are from theoretical calculation. See SI for images of spin-dependent OSH shifts.

The weak value of transverse shift, post-selected at a retardance Γ, is readily obtained.

$$\delta y_w(\Gamma) = \frac{\langle \psi(\Gamma)|\, metaOSH\, |P_1\rangle}{\langle \psi(\Gamma)|\, P_1\rangle} = \frac{z}{z_0}\cdot \delta y \cdot \tan\left(\pi\Gamma\right) \tag{3}$$

Note that the phase retardance $\Gamma = \frac{1}{2} \pm \varepsilon$ $(0 < \varepsilon \ll 1)$ is the range where a weak measurement amplification is achieved. In Fig. 3(b) is plotted the transmitted light intensity through the cross polarizer/analyser setup of Fig. 3(a) as a function of retardance Γ. Figure 3(c) shows the weak value, $\delta y_w(\Gamma)$, of an optical beam normally incident on PMS as a function of retardance Γ along with the corresponding transverse shift δy. At $\Gamma = 1/4$ the weak value $\delta y_w(\Gamma = 1/4) = 7.44\mu m$, which corresponds to the transverse shift $\delta y = 124nm$ in the absence of cross-polarized polarizer/analyzer. It is important to note that the phase-retardance dependent weak value is measured in the far field. [19–21]

Since the weak value is post-selected at phase retardance Γ, an electric manipulation of phase

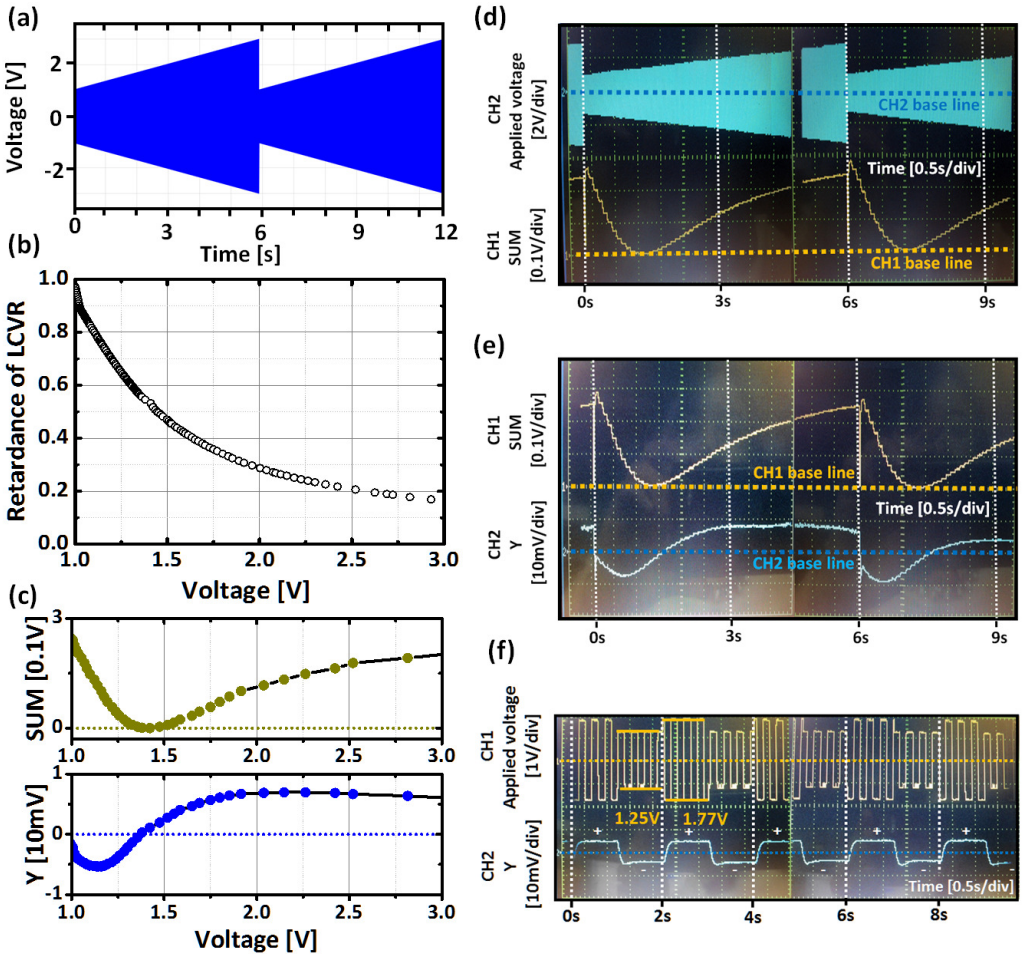


Fig. 4. (a) Saw-tooth waveform of LCVR driving voltage is plotted. (b) Retardance of LCVR and (c) SUM and Y of PSD are plotted as a function of LCVR driving voltage. Oscilloscope traces of (d) saw-tooth waveform and SUM of PSD and (e) SUM and Y of PSD are shown. (f) Switching between positive and negative Y is demonstrated as driving voltage is varied.

retardance in LCVR allows a control of the weak value δy_w.

Figure 4 shows plots and oscilloscope traces of OSH shift control. A saw-tooth waveform of LCVR driving voltage is adopted with $1.0V$ and $3.0V$ as the initial and final voltages, which covers the phase retardance from 0 to 1 (modulus of π). From a position-sensitive detector (PSD), SUM $=q_1+q_2+q_3+q_4$ and Y$=(q_1+q_2)-(q_3+q_4)$ are monitored, where Y is associated with OSH shift.

Comparison of Fig. 4 (b) and (c) shows that a sign reversal in Y takes place across the phase retardance $\Gamma=\frac{1}{2}$, at the vicinity of which a weak measurement amplification is achieved shown in Fig. 3(b) and (c). This leads to a switching behavior of post-selected OSH transverse shift when the phase retardance is varied crossing $\Gamma=\frac{1}{2}$. In Fig. 4(f) is demonstrated a switching between positive and negative Y as the driving voltage is alternated between $1.25V$ ($\Gamma=0.65$)

and $1.77V$ ($\Gamma = 0.35$). Switching operation of post-selected OSH shift has a strong implication in nanoscale photonics applications such as angular momentum transfer and sensing.

Methods

Sample fabrication. Phase-discontinuity metasurface is composed of V-shape antenna pattern. [2] A linear array of eight V-shape apertures is repeated along x-axis with the lattice constant Γ of 2400nm. Focused ion beam milling is utilized to fabricate Babinet complementary V-shaped antennas on e-beam evaporated 30nm-thick Au film on top of fused silica substrate with adhesion layer of 3nm thick titanium. [18]

Experimental set-up. We adopted $10mW$ $\lambda = 1310nm$ pigtail style self-contained thermally stabilized laser diode as the light source (OZ optics-OZ-2000) with the output fiber diameter 50 μm. The beam passes through a Glan/Thomson polarizer $P1$ (Thorlabs-GL10-C) to be linearly polarized. Then it is focused onto the metasurface with a microscope objective lens, $f = 95mm$, to a $1/e^2$ intensity spot size w_0 = $50\mu m$. The extraordinary refraction beam is collected with a microscope objective lens, $f = 95mm$, and a liquid crystal variable retarder (Thorlabs-LCC1113-C) and a second polarizer $P2$ are adopted to resolve the polarization state with an InGaAs-based NIR camera (Ophir-XC-130), and InGaAs-based quadrant position sensitive detector (Newport-2903) with a 3-mm diameter active region is employed for imaging and detection. In our experimental set-up, the propagation distance is $z = f = 60\, z_0$. Position sensitive detector is connected to the oscilloscope, and the position X, Y, and SUM data are monitored. The relative transverse shift [nm] $= (Y_{\sigma^+}/SUM_{\sigma^+} - Y_{\sigma^-}/SUM_{\sigma^-}) \times 1.08 \times beam\ radius\ [nm]$, which is obtained from the light intensity measurement by a photo-reciver placed on two dimensional translation stage.

Acknowledgement This work is supported by Quantum Metamaterial Research Center program and Global Frontier Program of Center for Advanced Meta-Materials (Ministry of Science, ICT and Future Planning, National Research Foundation, Republic of Korea).

SUPPLEMENTARY INFORMATION

Control of optical spin Hall shift in phase-discontinuity metasurface by weak value measurement post-selection

Y.U. Lee and J.W. Wu

Supplementary information consists of S1. Derivation of OSH shift in terms of Berry connections in PMS and S2. Images of spin-dependent OSH shifts.

S1. Derivation of OSH shift in terms of Berry connections in PMS

The transverse shift upon refraction has been related to the Berry connection. [22, 23]

$$\delta y = \langle z^i \,|\Lambda_{k^i}|\, z^i\rangle - \langle z^t \,|\Lambda_{k^t}|\, z^t\rangle \tag{4}$$

where $|z^{t,i}\rangle$ and $\Lambda_{k^{t,i}}$ stand for polarization state and Berry connection of refraction and incidence beams. Bliokh *et al*. expressed the Berry connection $\hat{A}^{(\lambda)}$ in terms of rectangular components of the linear momentum to obtain OSH shift δy of optical beam with spin λ. [23] For PMS surface, we have

$$\begin{aligned}
\delta y &= \hat{A}^{(\lambda)}_{iy} - \hat{A}^{(\lambda)}_{ty} \\
&= \lambda\left(\frac{p_{tx}p_{tz}}{p_t(p_{tx}^2+p_{ty}^2)} - \frac{p_{ix}p_{iz}}{p_i(p_{ix}^2+p_{iy}^2)}\right) \\
&= \lambda\left(\frac{p_{tz}}{p_t p_{tx}} - \frac{p_{iz}}{p_i p_{ix}}\right) \\
&= -\lambda\frac{\cos\theta_t - \cos\theta_i}{|\nabla\Phi|}
\end{aligned} \tag{5}$$

where $p_{tx} = -\hbar|\nabla\Phi|,\ p_{tz} = \hbar k_t\cos\theta_t,\ p_i = p_t = \hbar k_i = \hbar k_t,\ p_{ix} = -\hbar|\nabla\Phi|,\ p_{iz} = k_i\cos\theta_i$, $\nabla\Phi = -|\nabla\Phi|\hat{x}$, and it is noted that $p_{iy} = p_{ty} = 0$.

S2. Images of spin-dependent OSH shifts

In order to obtain images of spin-dependent OSH shifts we employed InGaAs-based NIR camera. After two separate measurements of I_{σ^+} and I_{σ^-}, we calculated $S_3 = \left(I_{\sigma^+} - I_{\sigma^-}\right)/\left(I_{\sigma^+} + I_{\sigma^-}\right)$ from each pixel signals. We examined how OSH shift behaves for *s*-polarization (*y*-polarization) and *p*-polarization (*x*-polarization) of extraordinary refraction beam. In Fig. 5 (a) blue and red solid circles correspond to *s*-polarization (*y*-polarization) and *p*-polarization (*x*-polarization), respectively. As shown in Fig. 5 (b) and (c), the relative transverse shifts show a sign reversal with the same magnitude, which is different from those observed in air-glass interface.

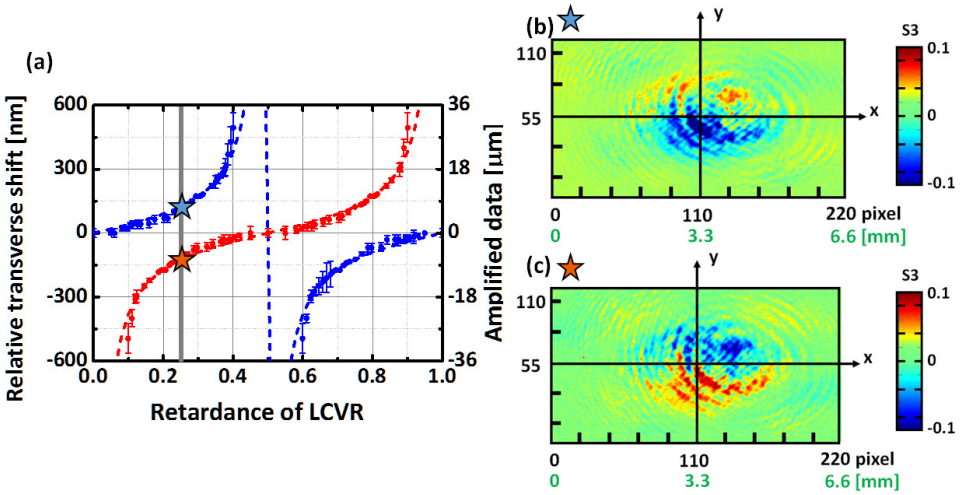


Fig. 5. (a) Relative transverse shifts are measured as a function of retardance Γ in cross-polarized polarizer/analyser setup (blue solid circles) and in parallel-polarized polarizer/analyser setup (red solid circles). Images of spin-dependent OSH shifts at $\Gamma = 1/4$ (vertical gray straight line in (a)) are obtained by processing each pixel signals in InGaAs-based NIR camera for (b) cross-polarized polarizer/analyser setup, $P_1 = (1,0)^T$ and $P_2 = (0,1)$, and (c) parallel-polarized polarizer/analyser setup, $P_1 = (0,1)^T$ and $P_2 = (0,1)$.

References and links

1. O. Hosten and P. Kwiat, "Observation of the spin Hall effect of light via weak measurements," Science **319**, 787–790 (2008).
2. N. Yu, P. Genevet, M. A. Kats, F. Aieta, J.-P. Tetienne, F. Capasso, and Z. Gaburro, "Light propagation with phase discontinuities: generalized laws of reflection and refraction," Science **334**, 333–337 (2011).
3. X. Yin, Z. Ye, J. Rho, Y. Wang, and X. Zhang, "Photonic spin Hall effect at metasurfaces," Science **339**, 1405–1407 (2013).
4. F. I. Fedorov, "Theory of total reflection," Dokl. Akad. Nauk SSSR **105**, 465?–468 (1955).
5. C. Imbert, "Calculation and experimental proof of the transverse shift induced by total internal reflection of a circularly polarized light beam," Physical Review D **5**, 787 (1972).
6. M. Onoda, S. Murakami, and N. Nagaosa, "Hall effect of light," Physical Review Letters **93**, 083901 (2004).
7. K. Y. Bliokh, A. Niv, V. Kleiner, and E. Hasman, "Geometrodynamics of spinning light," Nature Photonics **2**, 748–753 (2008).
8. M. Berry, "The quantum phase, five years after," in "Geometric phases in physics," , D. L. Andrews and M. Babiker, eds. (World Scientific Singapore, 1989).
9. V. Liberman and B. Y. Zeldovich, "Spin-orbit interaction of a photon in an inhomogeneous medium," Physical Review A **46**, 5199 (1992).
10. R. Y. Chiao and Y.-S. Wu, "Manifestations of Berry's topological phase for the photon," Physical Review Letters **57**, 933–936 (1986).
11. M. Onoda, S. Murakami, and N. Nagaosa, "Geometrical aspects in optical wave-packet dynamics," Physical Review E **74**, 066610 (2006).
12. K. Y. Bliokh, "Geometrodynamics of polarized light: Berry phase and spin Hall effect in a gradient-index medium," Journal of Optics A: Pure and Applied Optics **11**, 094009 (2009).
13. K. Y. Bliokh and V. Freilikher, "Topological spin transport of photons: Magnetic monopole gauge field in Maxwell's equations and polarization splitting of rays in periodically inhomogeneous media," Physical Review B **72**, 035108 (2005).
14. N. Ritchie, J. Story, and R. G. Hulet, "Realization of a measurement of a weak value," Physical Review Letters **66**, 1107 (1991).
15. M. R. Dennis and J. B. Götte, "The analogy between optical beam shifts and quantum weak measurements," New Journal of Physics **14**, 073013 (2012).

16. G. Jayaswal, G. Mistura, and M. Merano, "Observation of the Imbert–Fedorov effect via weak value amplification," Optics Letters **39**, 2266–2269 (2014).
17. F. Töppel, M. Ornigotti, and A. Aiello, "Goos–hänchen and Imbert–Fedorov shifts from a quantum-mechanical perspective," New Journal of Physics **15**, 113059 (2013).
18. Y. U. Lee, J. Kim, J. H. Woo, L. H. Bang, E. Y. Choi, E. S. Kim, and J. W. Wu, "Electro-optic switching in phase-discontinuity complementary metasurface twisted nematic cell," Optics Express **22**, 20816–20827 (2014).
19. Y. Gorodetski, K. Bliokh, B. Stein, C. Genet, N. Shitrit, V. Kleiner, E. Hasman, and T. Ebbesen, "Weak measurements of light chirality with a plasmonic slit," Physical Review Letters **109**, 013901 (2012).
20. J. Dressel, M. Malik, F. M. Miatto, A. N. Jordan, and R. W. Boyd, "Colloquium: Understanding quantum weak values: Basics and applications," Reviews of Modern Physics **86**, 307 (2014).
21. A. G. Kofman, S. Ashhab, and F. Nori, "Nonperturbative theory of weak pre-and post-selected measurements," Physics Reports **520**, 43–133 (2012).
22. M. Onoda, S. Murakami, and N. Nagaosa, "Geometrical aspects in optical wave-packet dynamics," Physical Review E **74**, 066610 (2006).
23. K. Y. Bliokh and V. Freilikher, "Topological spin transport of photons: Magnetic monopole gauge field in Maxwell's equations and polarization splitting of rays in periodically inhomogeneous media," Physical Review B **72**, 035108 (2005).